Supporting Information

RuO_{2-x} Decorated $CoSnO_3$ Nanoboxes as High Performance Cathode Catalyst of Li–CO_2 Batteries

Guanghui Yue [a*], Xianrui Luo [a], Zhenyu Hu [a], Wanjie, Xu [a], Jintang Li [a], Jinzhang Liu[b], Ruiguo Cao [c*]

[a] Department of Materials Science and Engineering, Xiamen University, Xiamen 361005, China

[b] School of Materials Science and Engineering, Beihang University, Beijing 100083 China

[c] Department of materials science and engineering, University of Science and Technology of China, Hefei, 230026, China

---

*Corresponding author: yuegh@xmu.edu.cn (G. H. Yue), rgcao@ustc.edu.cn (Ruiguo Cao). Tel: 86-592-2180155; Fax: 86-592-2183515

1. Experimental section

1.1 Synthesis of hollow $CoSnO_3$ nanoboxes

The hollow $CoSnO_3$ nanoboxes were synthesized as our previously reports [1]. Representatively, as the OH^- were instilled into the mixed aqueous solution, the $CoSn(OH)_6$ nanocubes were formed with the Co^{2+} and Sn^{4+} by a fast stoichiometric coprecipitation method. Following with excess OH^-, the $CoSn(OH)_6$ nanocubes were being translated into the porous $CoSn(OH)_6$ nanoboxes (Fig. S1) by an alkaline etching process. Finally, the heterogeneous and porous $CoSnO_3$ nanoboxes with amorphous structure were gated by a thermally induced dehydration mechanism in the argon atmosphere.

1.2 Synthesis of RuO_{2-x} nanoparticles decorated $CoSnO_3$ nanoboxes

The self-assembled liquid-plasma appliance was used to synthesize the RuO_{2-x} nanoparticles decorated $CoSnO_3$ nanoboxes nanocomposites (the appliance was shown in Fig. S2). Fistly, the as synthesized $CoSnO_3$ nanoboxes were added into the $RuCl_3$ solution. Then, the pH value of the mixed solutions were adjusted to 9 using sodium hydroxide. Next, 50 ml the mixed solutions were suffered a liquid-plasma course with a pulse voltage and discharge current are 500 mA for 2 min. Finally, the end-product $CoSnO_3/RuO_{2-x}$ nanocomposites were collected by centrifugation, rinsed with the deionized water and ethanol and then stoved at 65 °C for 10 h.

Here, 0.1g $CoSnO_3$ nanoboxes dispersed into the difference in concentrations of the 3 mL $RuCl_3$ solution, the concentrations as 0, 5, 10 and 20 mg/mL, respectively. And in this manuscript, most of the results were accord the samples which prepared with the concentrations of the $RuCl_3$ solution is 10 mg/mL, unless explicitly stated.

1.3 Characterization of materials

The crystal phase components of the samples were examined by X-ray diffraction (XRD, Bruker D8 with Cu K_{α} Radiation 40kV, 40mA). Morphologies and structures of the end-products were detected by scanning electron microscopy (SEM, LEO-1530) and transmission electron microscopy (TEM, JEM-2100, 200 kV). The composition and the chemical state of the obtained products were recorded using X-ray photoelectron spectroscopy (XPS PHI QUANTUM 2000 with monochromatic Al K X-ray source). Raman spectra were implemented and collected using a 632.8 nm laser with Jobin-Yvon Raman system. TriStar 3020 system was used to detect the N_2 absorption–desorption examinations.

1.4 Battery assemblies and electrochemical tests

Here, CR2032-type coin cells were assembled and applied to detect the electrochemical performances of the Li–CO_2 batteries. A slurry, mixed with the active materials, Ketjen black carbon and polyvinylidene difluoride (PVDF) with a weight ratio of 6:3:1, was spin-coated on a tailored carbon paper and then baked at 80 °C for 12h with a vacuum oven. The mass loading of the above-mentioned mixture was about 1.0-1.3 $mg \cdot cm^{-2}$. The cells were fabricated in an argon filled glove box (<0.1 ppm of H_2O and <0.1 ppm of O_2). A lithium plate was used as the counter electrode and separator was a Whitman glass microfiber separator filled with electrolyte. The electrolyte was 150 μL of 1M LITFSI (lithium bis-(trifluoromethanesulfonyl)-imide) in TEGDME (tetraethylene glycol dimethyl ether). The assembled cells were putted in a chamber filled with pure CO_2 (99.999%) for testing. The NEWARE battery test system was implied to detect the galvanostatic electrochemical performance at different current densities. The potential range during the cycles was 2.0 V to 4.5 V. An auto-lab 302N electrochemical workstation conducted was used to test the CV curve at the range of 2.0–4.5 V with a sweep rate of 0.1 mV s^{-1}. For comparison, the electrochemical properties of $CoSnO_3$ nanocubes were also been measured. All the specific capacities during galvanostatic discharge/charge processed were calculated based on the mass of active materials.

2. Part of the experimental results and discussion

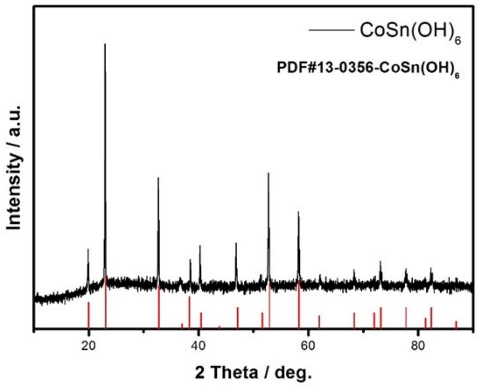

Figure S1. The XRD pattern of hollow structure $CoSn(OH)_6$ precursor.

It can be found that the diffraction peaks of the as synthesized precursor are good in accordance with the standard PDF card (PDF #13-0356), and this result indicated that the $CoSn(OH)_6$ precursor can be synthesized with the stoichiometric coprecipitation method.

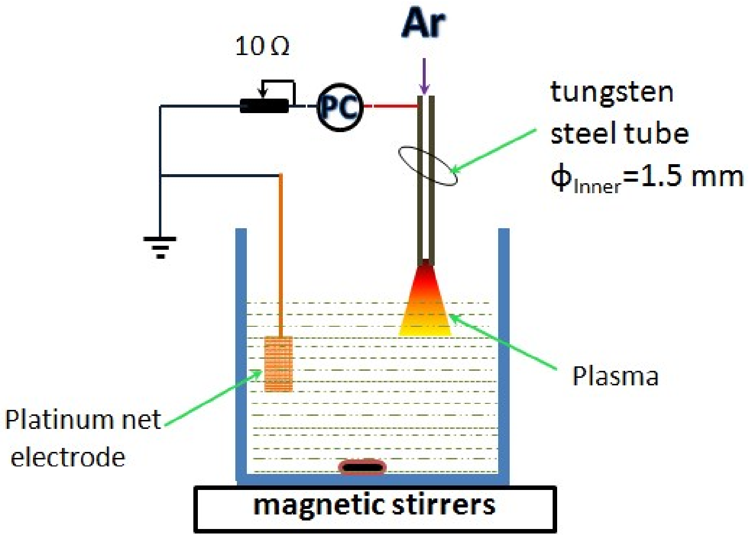

Figure S2. Schematic of the liquid-plasma experimental setup.

In this experiment, a platinum net (99.99%, 10 mm×10 mm) was immerged in the 50 mL mixed solution as one electrode. A tungsten steel tube was used as the other electrode in the atmospheric pressure to generate the argon plasma. The distance from the lower port of the tungsten steel tube to the electrolyte surface is about 3 mm. A high-power pulsed current source with a frequency of 5 kHz was implemented to the tungsten steel tube to generate the plasma. The current was adjusted with a 10 Ω current regulator. In our experiment, the discharge current detected was 500 mA in peak-to-peak value which was helpful to generate sufficient reducible reactive species in short time. As the effect by the plasma, the output voltage became distorted and looked like a bipolar pulse DC voltage which was applied to RuO_{2-x} formation.

In general, many short- and long-lived reactive species could be generated during the liquid-plasma interaction. These reactive species with a wide range of redox potential from -2.87 eV to +2.85 eV entered into the liquid to form a thinner layer on the liquid surface which included the short-lived reactive species (hydrated electron, atomic hydrogen etc.). And more importantly, a bulk of plasma zone could be formed as a plasma-affected liquid zone with the long-lived reactive species (hydrogen molecule, hydrazine etc.) which did great favorable for the Metal ions reducing [2-4]. On account of the electrochemistry, the RuO_{2-x} synthesis mechanism was inferred as followings:

$$Ru^{3+}\,(liq) + OH^{-}\,(liq) + e^{-}\,(liq) \Rightarrow Ru(OH)_3^{-}\,(liq) \quad \text{L L L L L L} \ (1)$$

$$Ru(OH)_3^{-}\,(liq) + X\,(liq) + H^{-}\,(liq) \Rightarrow RuO_{2-x}\,(sol) + Y^{Z} \quad \text{L L L L} \ (2)$$

Here, the X is the reducing species (e.g., hydrated electron), and Y is the product of the reaction between $Ru(OH)_3^{-}$ and X, and Z is the charge possessed by Y, depending on the charge possessed by X [2].

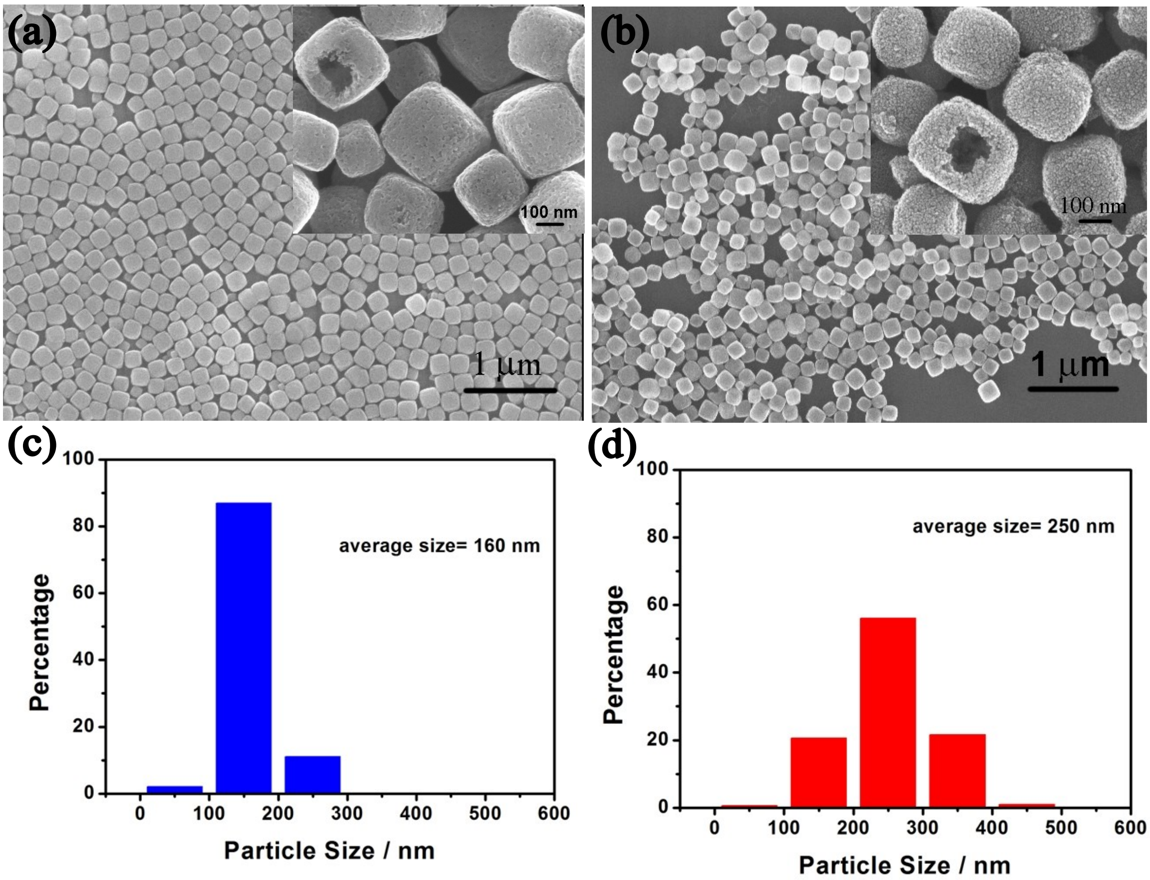

Figure S3. The SEM images and corresponding size distribution patterns of (a, c) $CoSnO_3$ nanoboxes, (b, d) the nanocomposites of the RuO_{2-x} decorated $CoSnO_3$ nanoboxes.

Fig. S3 revealed the SEM images of the bare $CoSnO_3$ nanoboxes and the nanocomposites which were decorated with the RuO_{2-x} nanoparticles on the surface of the hollow $CoSnO_3$ nanoboxes, respectively. It was obvious that the bare $CoSnO_3$ nanocubes were uniform nanocubes with an average size about 160 nm. The hollow structure nanoboxes could be confirmed with the broken cubes (inserted in Fig. S3). Compared with the smooth surface of the bare $CoSnO_3$ nanoboxes, the SEM image indicated that after the as synthesized bare $CoSnO_3$ nanoboxes were suffered with the liquid-plasma course in the mixed ruthenium chloride solution, the obtained products also implied a nanoboxes nanostructure, except the surface of nanoboxes were turned from initially smooth into rough. There are many small size nanoparticles were decorated on the surface of the bare nanoboxes. With the statistical results, it can be deduced that the average size distribution of nanoboxes was increased to 250 nm (Fig. S3d). Here, the average size distribution increasing would be attributed to the superficial nanoparticles which with small size were grown and decorated on the surface of the bare $CoSnO_3$ nanoboxes.

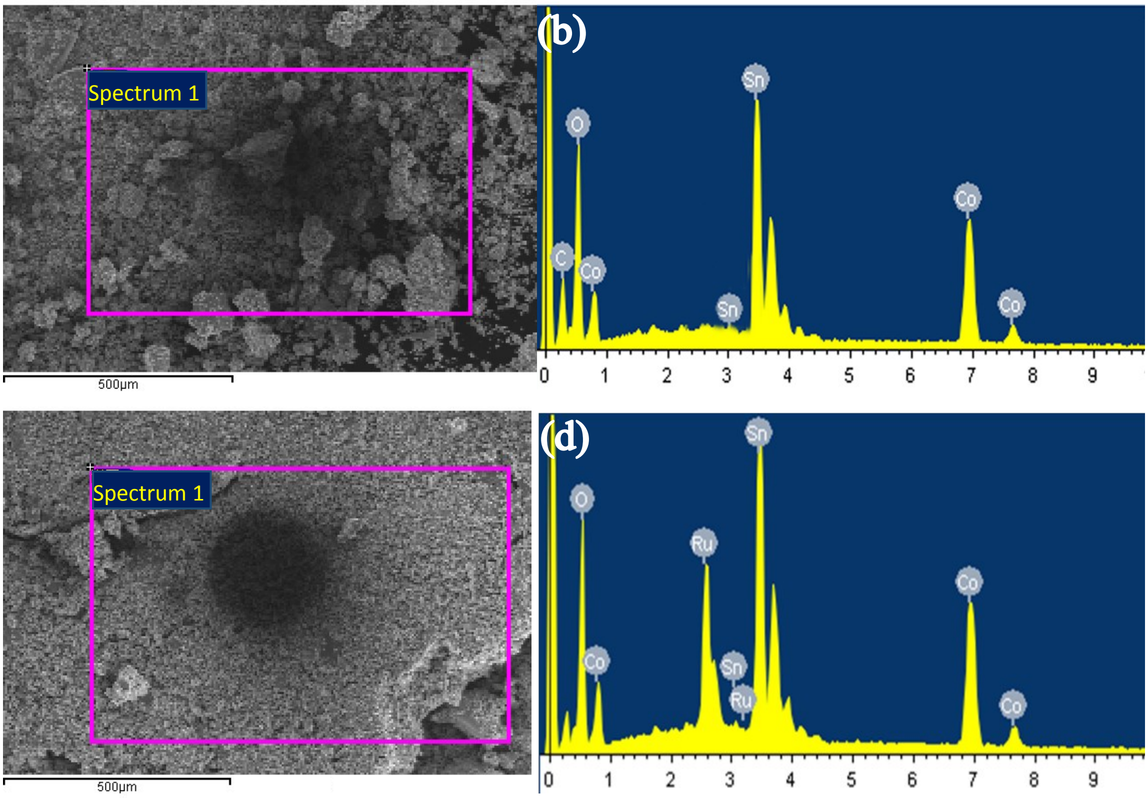

(e)

	$CoSnO_3$		$CoSnO_3/RuO_{2\text{-}x}$ nanocomposites	
Element	**Weight%**	**Atomic%**	**Weight%**	**Atomic%**
C K	3.21	8.11	3.13	8.66
O K	37.61	71.31	32.37	67.16
Co K	21.05	10.84	20.89	11.77
Sn L	38.13	9.74	39.14	10.95
Ru L			4.47	1.46
Total	**100**		**100**	

Figure S4. The SEM-EDX pattern of the $CoSnO_3$ nanoboxes (a & b) and $CoSnO_3/RuO_{2\text{-}x}$ nanocomposites (c & d). And the composition of the $CoSnO_3$ nanoboxes and $CoSnO_3/RuO_{2\text{-}x}$ nanocomposites (e), respectively.

Fig. S4 revealed that the elements of the cobalt, tin, ruthenium, and oxygen could be verified with the energy-dispersive X-ray spectroscopy (EDX) images, and the ratio of the metallic element (cobalt: tin: ruthenium) was about 11.77:10.95: 1.46, which indicated that there is only a little ruthenium elements were decorated on the surface of the bare $CoSnO_3$ nanoboxes to forming the $CoSnO_3/RuO_{2-x}$ nanocomposites.

The inductively coupled plasma atomic emission spectroscopic (ICP) analysis and EDX results of the samples which were synthesized with different $RuCl_3$ concentrations were shown in the table 1 and 2.

Table 1 the composition of the $CoSnO_3/RuO_{2-x}$ nanocomposites synthesized with different $RuCl_3$ concentrations.

Samples No.	Concentrations of the $RuCl_3$ solution (mg/mL)	ICP results (Atomic%) Co:Sn:Ru	EDX results (Atomic%) Co:Sn:Ru
1	0	10.97:9.62 (Co:Sn)	10.84:9.74 (Co:Sn)
2	5	12.35:12.04:0.76	12.25:11.54:0.81
3	10	11.45: 11.21:1.51	11.77:10.95: 1.46
4	20	10.25:9.75:1.84	10.85:10.23:1.77

Note: The sample 3 is the main sample with the best electrochemical performance and named as $CoSnO_3/RuO_2$ nanocomposites.

Table 2 ICP results (Atomic%) for the $CoSnO_3/RuO_{2-x}$ nanocomposites synthesized with different $RuCl_3$ concentrations.

Samples No.	Concentrations of the $RuCl_3$ solution (mg/mL)	ICP results (Atomic%) Co:Sn:Ru:O
1	0	10.97:9.62:30.86 (Co:Sn:O)
2	5	12.35:12.04:0.76:36.72
3	10	11.45: 11.21:1.51:34.41
4	20	10.25:9.75:1.84:30.56

From this table, it can be detected that the molar ratio between metal elements and the oxygen is 0.667, 0.685, 0.711 and 0.725. Since there with any different of the XPS measurement of the bare sample of $CoSnO_3$, we can calculate that the molar ratio between Ru and O is much larger than 0.5. So, it can be inferred that there are some oxygen vocation existed in our samples.

For example to calculate the molar ratio between Ru and O with sample No.2:

Metal:O in sample No.1: (10.97+9.62)/30.86=0.667

O Molars in sample No.2 :Metal(Sn and Co): (12.35+12.04)/0.667=36.57

O Molars matched to Ru in sample No.2: 36.72-36.57=0.15

Ru:O in sample No.2: 0.76/015=5» 0.5 (stoichiometric ratio)

In addition, a weight loss of the TG curve before 100 ℃ can be inferred as the absorbed water from the air. The TG curve indicated an increase in weight from the 100 ℃ to 200 ℃, which can be attributed to a oxidation reactions, in other words, the RuO_{2-x} had been oxidized into RuO_2. I think this phenomenon can explain that there are some oxygen vacancy existed in the $CoSnO_3/RuO_{2-x}$ nanocomposites from a side.

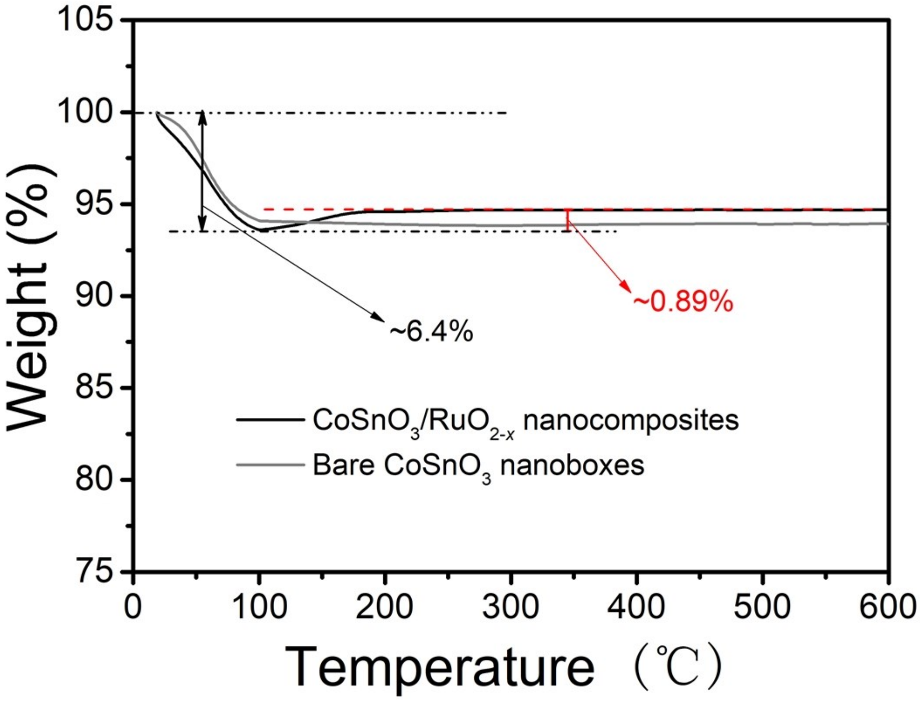

Fig. S5 The TG curves of the as synthesized $CoSnO_3$ nanoboxes and the $CoSnO_3/RuO_{2-x}$ nanocomposites.

XPS measurement was carried out to further determine the element species and the element valences of the as prepared bare $CoSnO_3$ nanoboxes and the $CoSnO_3/RuO_2$ nanocomposites. Fig. S6 exhibited the XPS spectrum of the as synthesized bare $CoSnO_3$ nanoboxes and the bare $CoSnO_3$ nanoboxes which had been dealt with the liquid-plasma course. All of the Co, Sn, C and O elements were detected in the full spectrum in the Fig. S6a, and there was no significant difference can be surveyed between the samples before and after the liquid-plasma course. A high resolution scans of the Co 2p, Sn 3d and O 1s peaks were illustrated in the Fig. S5(b-d), respectively. In the Fig. S6b, two distinct and glabrous peaks located at 781.2

and 795.7 eV, which could be assigned to the Co $2p_{3/2}$ and Co $2p_{1/2}$ of the Co^{2+}, which are in good agreement with previous reports [5-7]. Fig. S6c illustrated a typical Sn 3d spectrum, two very specific and sharp peaks appeared at about 486.8 and 495.2 eV could be marked as Sn $3d_{5/2}$ and Sn $3d_{3/2}$, which were kept high conformity with the electronic state of the Sn^{4+} [8-11]. From the high resolution O 1s peak which was depicted in the Fig. S6d, it is easy to discovered that the peak was centered around 530.4 eV could be ascribed to the metal oxide form O^{2-} [6, 10]. But from Fig. S6d, it could be reconnoitred that the peak width had been broadened when the $CoSnO_3$ nanoboxes samples had been processed with the liquid-plasma course. In order to dig deeper to confirm the influence of the liquid-plasma course, Gaussian fitting method was used to analyze the O 1s spectrum of the $CoSnO_3$ nanoboxes samples after it had been dealt with the liquid-plasma course. As shown the inserted in the Fig S6d, the spectrum of the O 1s had been best fitted to two spin-orbit doublets characteristic, the peak detected at about 530.4 eV could be equivalent to the metal-oxygen bands form the $CoSnO_3$ nanoboxes, and the peak situated at around 532.0 eV was corresponds to the surface absorbed categories, which may be ascribed to the surface contaminates of the sample which had been exposed to the air conduction before all kinds of the measurement [6, 12, 13].

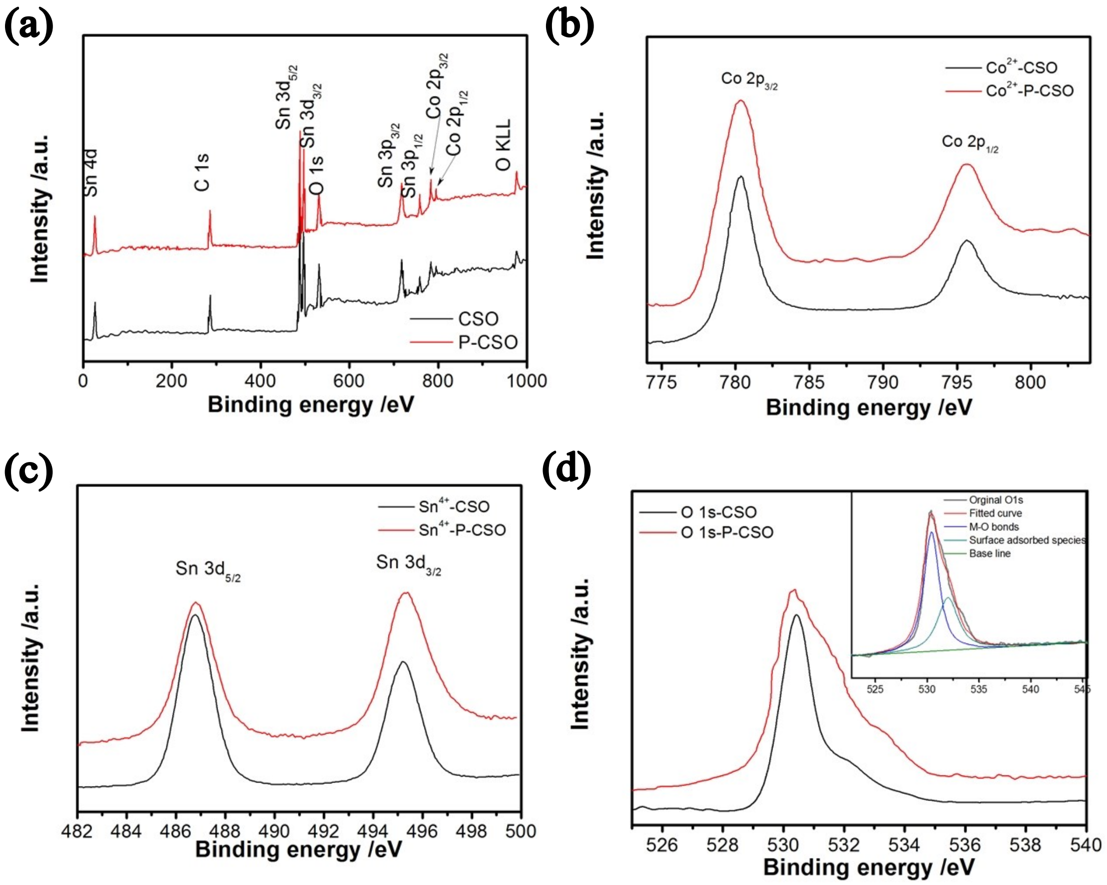

Fig. S6 The X-ray photoelectron spectra of the as synthesized $CoSnO_3$ nanoboxes (Marked as CSO with the black line) and the $CoSnO_3$ nanoboxes after suffering the liquid-plasma course (Marked as P-CSO with the red line).

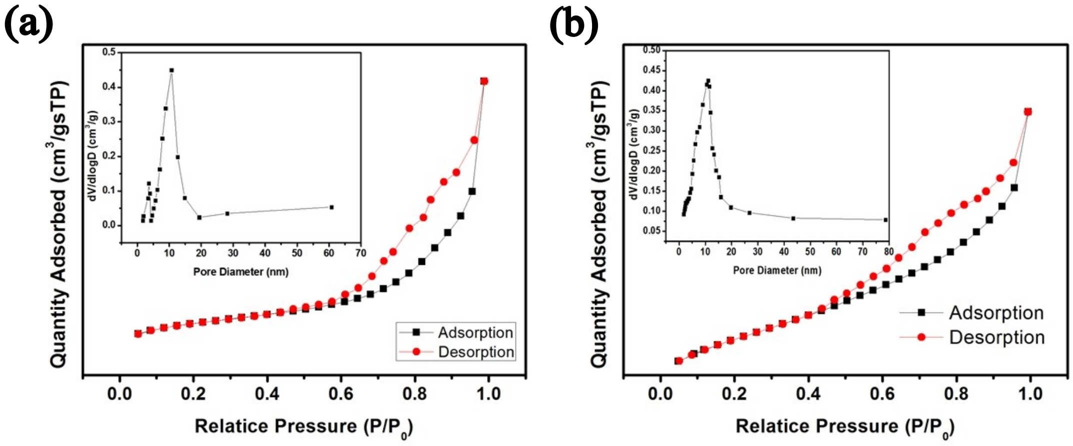

Figure S7. N_2 absorption-desorption profiles of $CoSnO_3$ nanoboxes (a) and $CoSnO_3/RuO_{2-x}$ nanocomposites (b) with corresponding pore size distribution (inset).

The specific surface areas of the $CoSnO_3$ nanoboxes and $CoSnO_3/RuO_{2-x}$ nanocomposites were detected to be 112.8 and 138.6 $m^2\ g^{-1}$, respectively. Both $CoSnO_3$ nanoboxes and $CoSnO_3/RuO_{2-x}$ nanocomposites indicated the mesoporous structure and the pores mainly center nearby 10.7 nm. There should be no doubt that $CoSnO_3/RuO_{2-x}$ nanocomposites displayed a larger specific surface area than $CoSnO_3$ nanoboxes. The higher specific surface area could supply more flexible response to the active site, larger contact area between electrode materials and electrolyte, which would improve the ORR/OER catalytic activity and promote the cycle performance of the Li-CO_2 batteries. And the porous feature of active particles could do great help for the diffusion of electrolyte and lithium ions within the electrode, which is helpful to strengthening the cycle performance. These merits make $CoSnO_3/RuO_{2-x}$ nanocomposites a very promising cathode material for next-generation lithium air batteries.

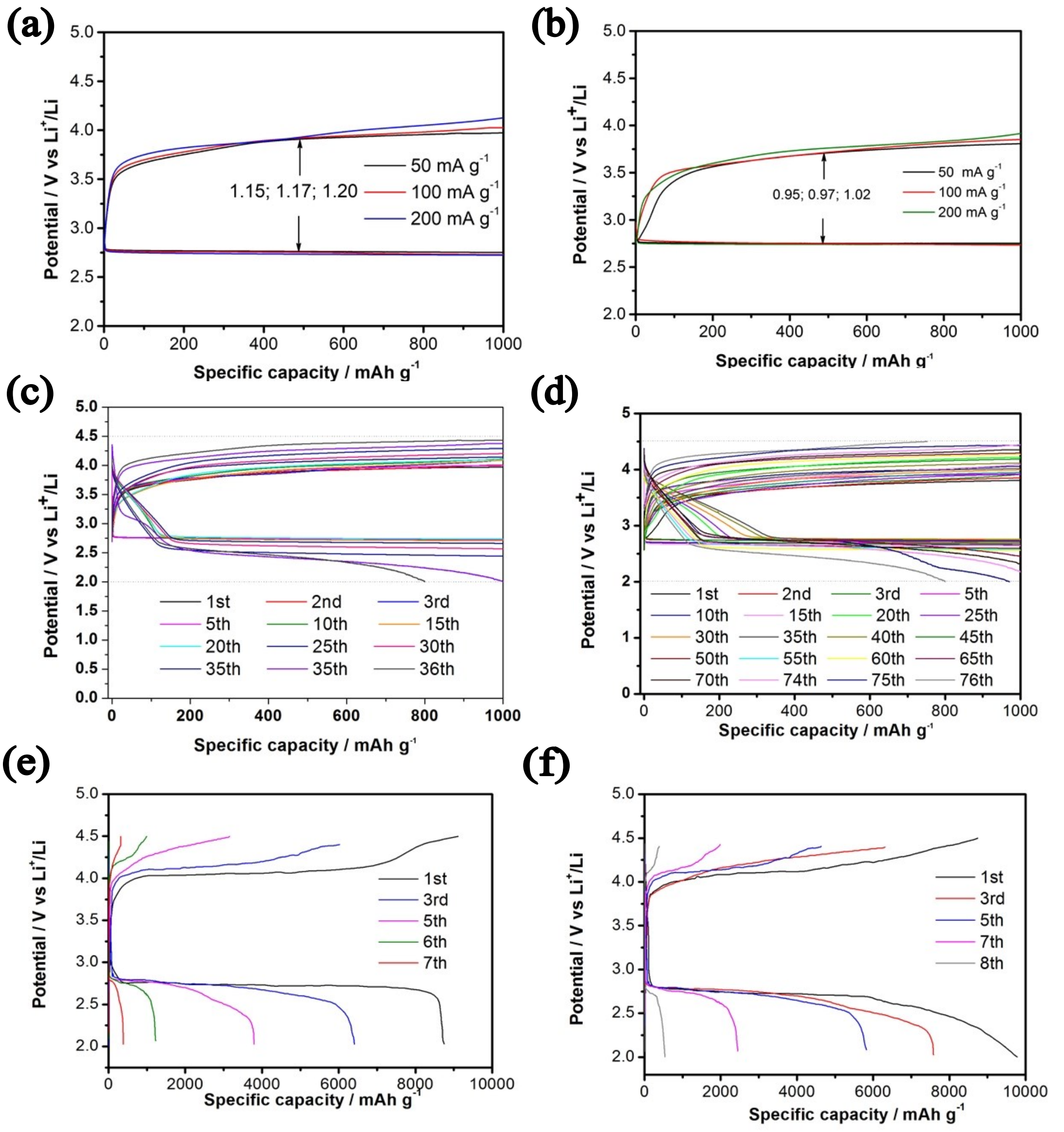

Figure S8. The discharge–charge profiles at current densities of 50, 100 and 200 mA g^{-1}, The full discharge/charge curves and the Cycling performance with $CoSnO_3$ nanoboxes cathodes at current density of 100 mA g^{-1} with a cut-off capacity of 1000 mAh g^{-1} of the $CoSnO_3$ nanoboxes cathodes (a, c, & e) and the $CoSnO_3/RuO_{2-x}$ nanocomposites cathodes (b, d, & f), respectively.

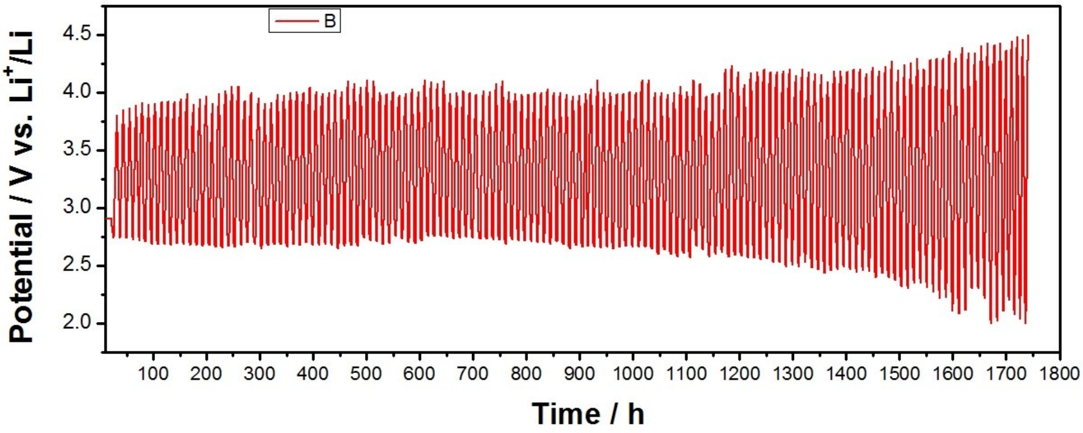

Figure S9. The full potential vs time curves of the battery with the $CoSnO_3/RuO_{2-x}$ nanocomposites as the cathodes.

In order to study the effect of the charge/discharge, the cycled cell were disassembled in the glove box and cleaned with the Dimethoxyethane (DMET) for several times and drying in vacuum for ex-suit XRD, Raman, SEM and XPS analyses.

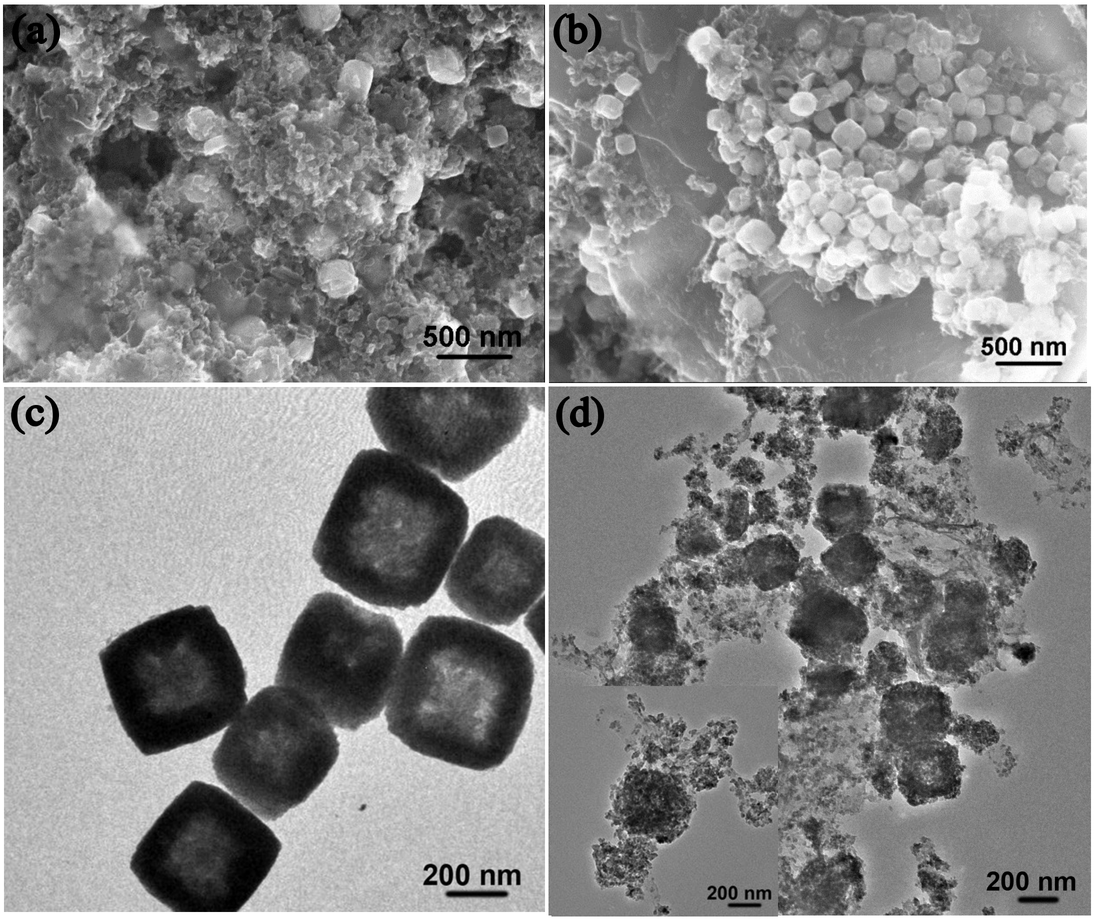

Figure S10. The SEM images of the $CoSnO_3/RuO_{2-x}$ nanocomposites cathodes after the 1st discharge (a) and recharge (b), respectively. The TEM image of the $CoSnO_3/RuO_{2-x}$ nanocomposites (c) and the TEM image of nanocomposites which were used as the cathode catalyst for 145 loops (d) , respectively.

After 145 loops, the surface of the nanoboxes were covered with the Li_2Co_3, the cubic-like morphology had been changed and it looks move closer to a spherical-like structure. Even more, they were pulverized into small nanoparticle with the magnitude of the surface tension that were derived from the iterative process, which is the nucleation growth and redecomposition of the lithium carbonate.

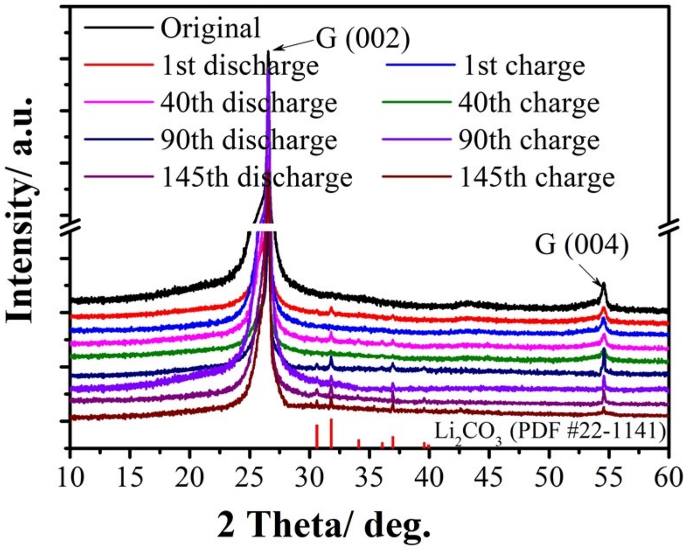

Figure S11. The full XRD spectrum of the $CoSnO_3/RuO_{2-x}$ nanocomposites cathodes with different discharge/charge.

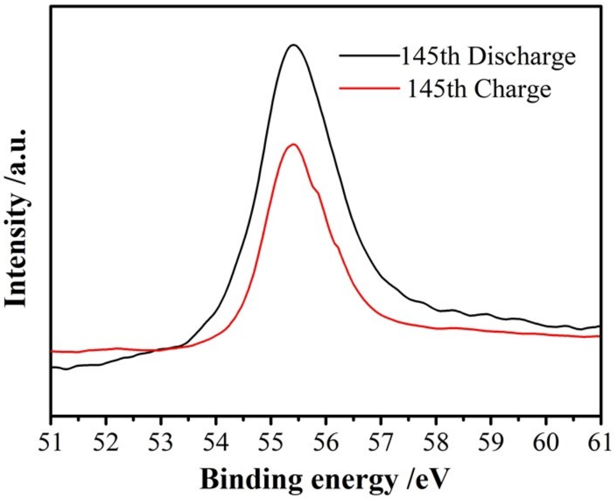

Figure S12. The XPS spectra of Li 1s for the $CoSnO_3/RuO_{2-x}$ nanocomposites cathodes after the 145th discharging/charging process.

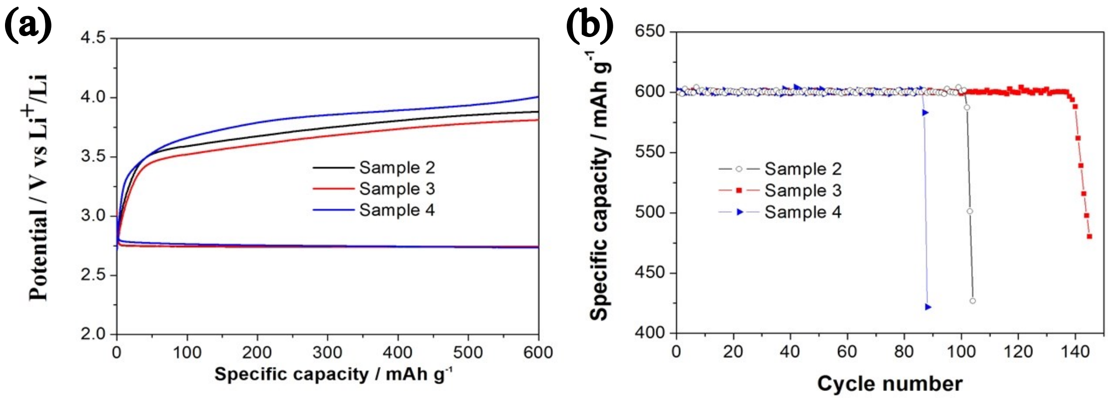

Figure S13. The first discharge–charge profiles at current densities of 200 mA g^{-1} for the samples which were prepared with different $RuCl_3$ concentrations. And the samples No. are corresponding to the table 1.

From this figure, it can be deduced that the sample 3 (Named as $CoSnO_3/RuO_{2-x}$ nanocomposites with the main results shown in the main manuscript) which synthesized with the $RuCl_3$ concentrations of 10 mg/mL indicated the lowest overpotential and the best cycle performance and the best clectrochemical catalysts performances and stability. So, in our manuscript, all the main results are tested with the sample 3.

References

[1] G.H. Yue, J. Liu, J. Han, D. Qin, Q. Chen, J. Shao, Chinese J. Catal., 39 (2018) 1951-1959.

[2] J. Liu, B. He, Q. Chen, H. Liu, J. Li, Q. Xiong, X. Zhang, S. Yang, G.H. Yue, Q. Liu, Electrochim. Acta, 222 (2016) 1677–1681.

[3] J.Liu, Q. Chen, J. Li, Q. Xiong, G.H. Yue, X. Zhang, S. Yang and Q. Liu, J. Phys. D: Appl. Phys. 49 (2016) 275201.

[4] Q. Chen, J. Li, and Y. Li, J. Phys. D: Appl. Phys. 48 (2015) 424005.

[5] Y. Cao, L. Zhang, D. Tao, D. Huo, K. Su, Electrochim. Acta, 132 (2014) 483-489.

[6] C. Guan, X. Li, H. Yu, L. Mao, L.H. Wong, Q. Yan, J. Wang, Nanoscale, 6 (2014) 13824-13830.

[7] X.X. Zhang, Q.S. Xie, G.H. Yue, Y. Zhang, X.Q. Zhang, A.L. Lu, D.L. Peng, Electrochim. Acta, 111 (2013) 746-754.

[8] X. Zhao, G. Wang, Y. Zhou, H. Wang, Energy, 118 (2017) 172-180.

[9] Z. Liu, R. Guo, J. Meng, X. Liu, X. Wang, Q. Li, L. Mai, Chem. Commun., 53 (2017) 8284-8287.

[10] L. Zhang, Y. Hu, J. Zheng, J. Mater. Chem. A, 5 (2017) 18664-18673.

[11] G. Zou, H. Hou, G. Zhao, P. Ge, D. Yin, X. Ji, J. Mater. Chem. A, 6 (2018) 4839-4847.

[12] J. Xu, L. He, W. Xu, H. Tang, H. Liu, T. Han, C. Zhang, Y. Zhang, Electrochim. Acta, 145 (2014) 185-192.

[13] L. Zhang, K. Zhao, R. Yu, M. Yan, W. Xu, Y. Dong, W. Ren, X. Xu, C. Tang, L. Mai, Small, 13 (2017) 1603973.